

Accepted Manuscript

Identification of a novel 5-amino-3-(5-cyclopropylisoxazol-3-yl)-1-isopropyl-1*H*-pyrazole-4-carboxamide as a specific RET kinase inhibitor

Hojong Yoon, Injae Shin, Yunju Nam, Nam Doo Kim, Kyung-Bok Lee, Taebo Sim



PII: S0223-5234(16)30912-6

DOI: [10.1016/j.ejmech.2016.10.050](https://doi.org/10.1016/j.ejmech.2016.10.050)

Reference: EJMECH 9015

To appear in: *European Journal of Medicinal Chemistry*

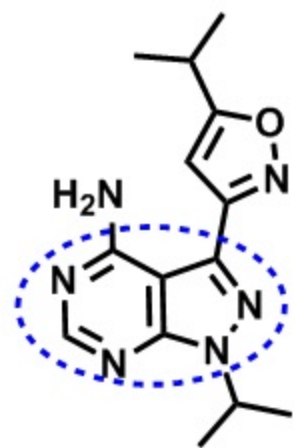
Received Date: 20 August 2016

Revised Date: 20 October 2016

Accepted Date: 21 October 2016

Please cite this article as: H. Yoon, I. Shin, Y. Nam, N.D. Kim, K.-B. Lee, T. Sim, Identification of a novel 5-amino-3-(5-cyclopropylisoxazol-3-yl)-1-isopropyl-1*H*-pyrazole-4-carboxamide as a specific RET kinase inhibitor, *European Journal of Medicinal Chemistry* (2016), doi: 10.1016/j.ejmech.2016.10.050.

This is a PDF file of an unedited manuscript that has been accepted for publication. As a service to our customers we are providing this early version of the manuscript. The manuscript will undergo copyediting, typesetting, and review of the resulting proof before it is published in its final form. Please note that during the production process errors may be discovered which could affect the content, and all legal disclaimers that apply to the journal pertain.



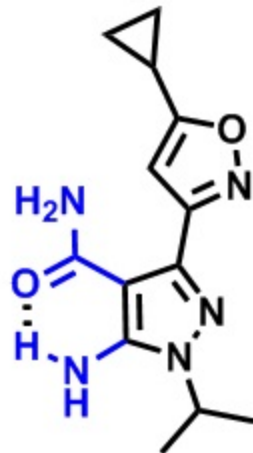
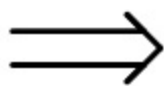
6g

Poor metabolic stability

wt-RET IC_{50} = 41 nM

V804M-RET IC_{50} = 355 nM

Scaffold hopping

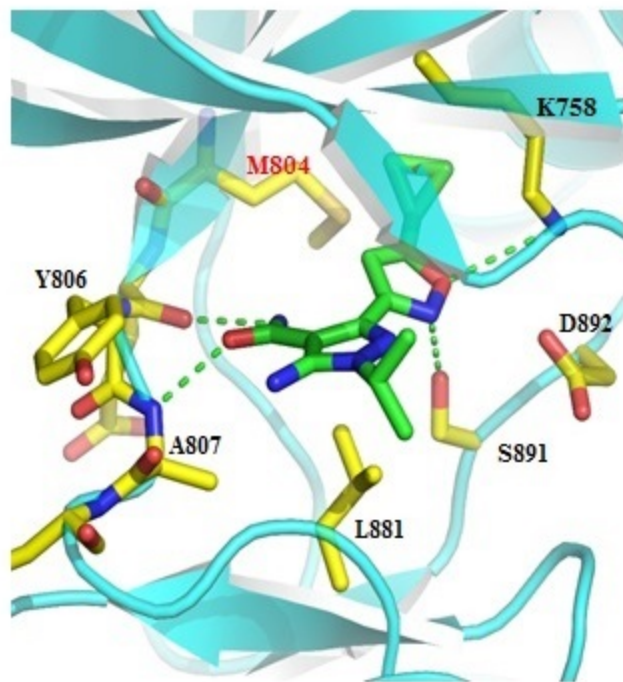


15l

Enhanced metabolic stability

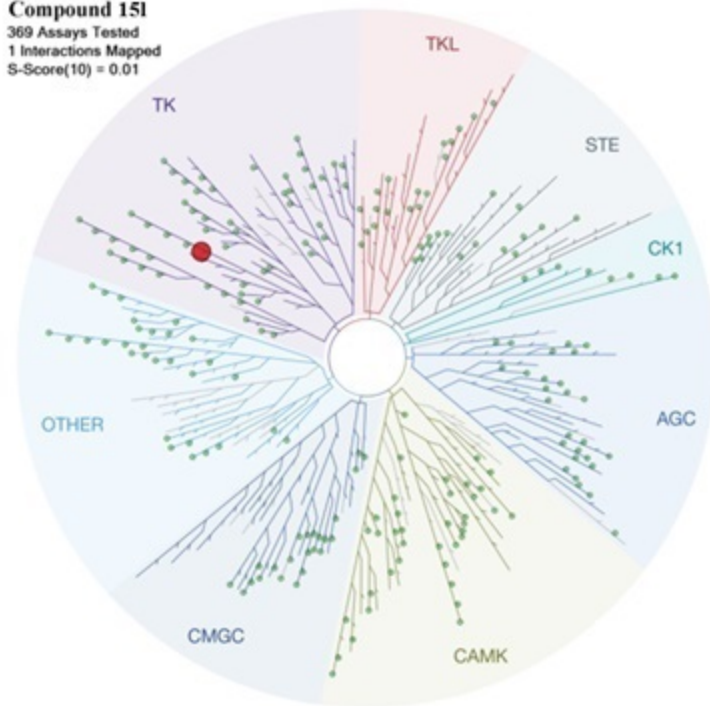
wt-RET IC_{50} = 44 nM

V804M-RET IC_{50} = 252 nM



Docking model of 15l on V804M-RET

Compound 15l
369 Assays Tested
1 Interactions Mapped
S-Score(10) = 0.01



Exceptional kinase selectivity

Identification of a novel 5-amino-3-(5-cyclopropylisoxazol-3-yl)-1-isopropyl-1*H*-pyrazole-4-carboxamide as a specific RET kinase inhibitor

Hojong Yoon^{a,1}, Injae Shin^{b,1}, Yunju Nam^b, Nam Doo Kim^c, Kyung-Bok Lee^d, Taebo Sim^{a,b,*}

^a *Chemical Kinomics Research Center, Korea Institute of Science and Technology (KIST), 5 Hwarangro 14-gil, Seongbuk-gu, Seoul 02792, Republic of Korea*

^b *KU-KIST Graduate School of Converging Science and Technology, Korea University, 145 Anam-ro, Seongbuk-gu, Seoul 02841, Republic of Korea*

^c *New Drug Development Center, Daegu-Gyeongbuk Medical Innovation Foundation, Daegu 41061, Republic of Korea*

^d *Division of Bioconvergence Analysis, Korea Basic Science Institute (KBSI), Daejeon 34133, Republic of Korea*

¹ *These authors contributed equally to this work.*

* Corresponding Author.

Dr. Taebo Sim

Chemical Kinomics Research Center, Korea Institute of Science and Technology (KIST), 5 Hwarangro 14-gil, Seongbuk-gu, Seoul 02792, Republic of Korea;

KU-KIST Graduate School of Converging Science and Technology, Korea University, 145 Anam-ro, Seongbuk-gu, Seoul 02841, Republic of Korea;

e-mail: tbsim@kist.re.kr; Tel.: +82-2-958-6437; Fax: +82-2-958-5549

Abstract

Activating mutations of REarrange during Transfection (RET) kinase frequently occur in human thyroid and lung cancers. An enormous effort has been devoted to discover potent and selective inhibitors of RET. Selective and potent inhibitors against constitutively active RET mutants are rare to date as identification of selective RET inhibitors is challenging. In a recent effort we identified a novel and specific RET inhibitor of 5-aminopyrazole-4-carboxamide scaffold, which was designed to enhance the metabolic stability of the pyrazolopyrimidine scaffold. In the SAR study described in the current report, we identified the 5-aminopyrazole-4-carboxamide analog **15I**, which displays high metabolic stability. Compound **15I** is potent against gatekeeper mutant ($IC_{50} = 252$ nM) of RET as well as against wild-type RET ($IC_{50} = 44$ nM). This substance effectively suppresses growth of Ba/F3 cells transformed with wild-type RET and its gatekeeper mutant (V804M), and thyroid-cancer derived TT cells while it does not affect parental Ba/F3 cells and Nthy ori-3-1, normal thyroid cells. Also, the results of a global kinase profiling assay on a panel of 369 kinases, show that **15I** exclusively inhibits RET. Based on its exceptional kinase selectivity, great potency and metabolic stability, **15I** represents a promising lead for the discovery of RET directed therapeutic agent and should be a key tool in studies aimed at understanding RET biology.

Keywords: RET kinase, metabolic stability, specific inhibitor, 5-aminopyrazole-4-carboxamide

1. Introduction

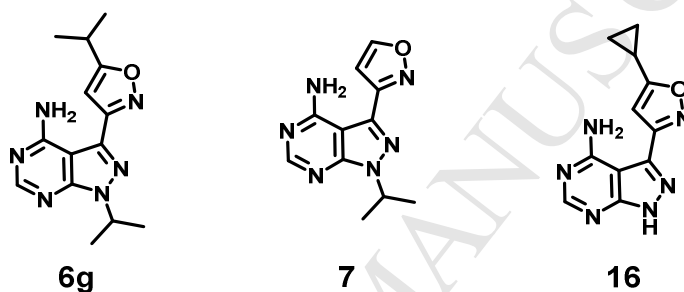
Among the more than 500 naturally occurring kinases that have been described thus far, several members are known to play important roles in a number of disease-related signaling pathways. Under normal conditions, kinases in cells are systematically regulated. Yet, aberrant kinase signaling taking place though overexpression or mutation results in a variety of cancers [1-3], inflammatory disease [4, 5] and complications of diabetes [6]. RET (REarrange during Transfection), one of the receptor tyrosine kinases, is crucial for the normal development, maturation and maintenance of tissues and

cells [7]. Deregulated RET signaling leads to familial and sporadic cancers, primarily medullary thyroid carcinoma (MTC) [7, 8]. The MTC family includes multiple endocrine neoplasia type 2A (MEN2A), type 2B (MEN2B) and familial thyroid carcinoma (FMTC), which are characterized by different RET missense mutations. MEN2A and FMTC are primarily associated with RET point mutations at Cys634 in the extracellular domain, which induce ligand-independent receptor dimerization via an illegitimate disulfide bond. This phenomenon results in constitutive RET signaling activation [9, 10]. MEN2B is caused by a M918T mutation in the substrate binding pocket, which promotes a conformational change that leads to constitutive kinase activity [11]. In addition, chimeric fusion proteins of RET with different exon genes such as KIF5B, CCDC6, TRIM33 or NCOA4 have been identified in non-small cell lung cancers (NSCLC). These proteins have been shown to lead to abnormal increases in RET transcription that cause tumorigenesis [12-15]. Owing to its role in aberrant signaling in thyroid carcinomas and NSCLC, RET is regarded as a promising target for the development of cancer therapeutic agents.

To date, various small molecule inhibitors of RET have been described including vandetanib (Caprelsa®), cabozantinib (Cometriq®), and lenvatinib (Lenvima®). Moreover, these RET kinase inhibitors have been clinically approved for the treatment of metastatic MTC or differentiated thyroid cancer (DTC). However, although exhibiting great clinical efficacy, these drugs elicit several acquired mutations and they are ineffective inhibitors against the gatekeeper mutants V804M and V804L [16, 17]. In an effort aimed at overcoming the resistance of the gatekeeper mutants of RET, we discovered that pyrazolo[3,4-*d*]pyrimidin-4-amine derivatives containing an isoxazole moiety serve as potent and selective RET kinase inhibitors [18]. Among these substances, **6g** (Figure 1) was shown to have a high RET kinase inhibitory activity ($IC_{50} = 41$ nM), However, the poor metabolic stability of **6g** in mouse liver microsomes (5.1% remaining after 15 min) impeded further biological evaluations such as its *in vivo* efficacy assessment (Figure 1A). To identify the source of the lability of **6g**, we measured the metabolic stability of the close pyrazolo[3,4-*d*]pyrimidin-4-amines analogues, **7** and **16**, which were selected to assess the respective influences of the substituent present on the isoxazole and pyrazole moieties of **6g**. Both compounds were found to display poor metabolic stability (2.6% and

1.4% remaining after 15 min, respectively) which suggests that the pyrazolo[3,4-*d*]pyrimidine or isoxazole heterocyclic moieties in **6g** are likely the source of its poor metabolic stability (Figure 2B). In the investigation described below, we tested this hypothesis using two types of variations involving a change of the isoxazole to an oxazole ring and a pyrimidine ring open strategy. This effort led to the discovery of the 5-aminopyrazole-4-carboxamide derivative **15l**, which is a specific and potent RET kinase inhibitor that has enhanced metabolic stability.

(A)



	6g	7	16
RET IC ₅₀ (μM)	0.041	0.213	0.052
Microsomal stability (% remaining, 15 min)	5.1	2.6	1.4

(B)

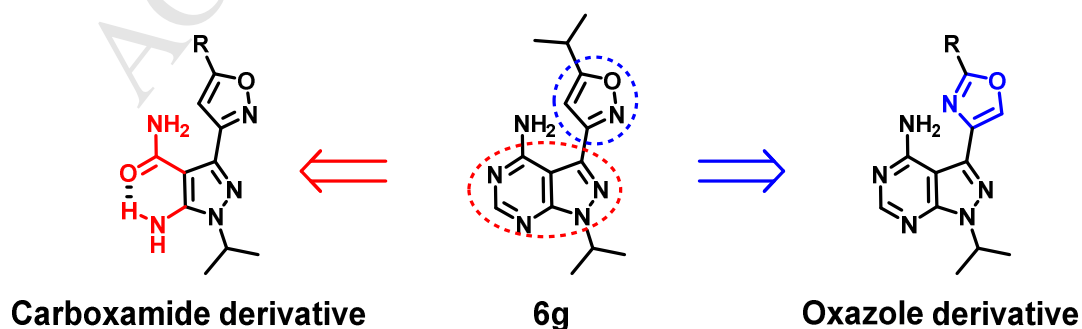
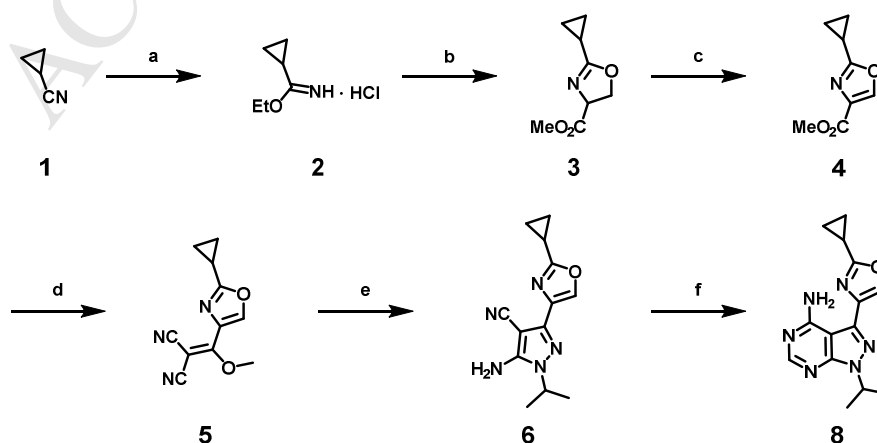


Figure 1. (A) Microsomal stability of pyrazolo[3,4-*d*]pyrimidin-4-amine derivatives containing an

isoxazole moiety. (B) Strategies to improve the microsomal stability of **6g**.

2. Results and discussion

As described above, an investigation was designed to determine if varying the nature of the isoxazole and 4-aminopyrimidine rings in **6g** would lead to an improvement in metabolic stability and retention of specific RET kinase inhibitory activity. Because pyrazolo[3,4-*d*]pyrimidine is an established scaffold for several kinase inhibitors including Ibrutinib, the FDA-approved drug [19, 20], our attention first focused on evaluating if the isoxazole ring in this substance is the main source of its poor metabolic stability. Moreover, isoxazoles are widely known to be the most readily cleaved heterocyclic ring system. For example, the N-O bond in this ring system is cleaved by photoisomerization [21], catalytic hydrogenolysis with Raney-Ni [22] or Pd/C [23], and reductive ring opening with transition metals such as molybdenum hexacarbonyl [Mo(CO)₆] [24]. Also, in terms of drug metabolism, cytochrome P450Fe(II) or NADH-dependent reductases promote isoxazole ring scission in leflunomide [25] and razaxaban [26] following their *in vivo* administration. In contrast, oxazoles are more stable than isoxazoles. Moreover, the oxygen atom in the oxazole ring is located at the same position as the isoxazole oxygen in **6g** and, as a result, hydrogen bonding interaction with Lys758 in the RET kinase domain would still exist [18]. Based on this information, we expected that replacement of the isoxazole in **6g** with an oxazole ring would lead to improved metabolic stability and retained inhibitory activity against RET kinase.

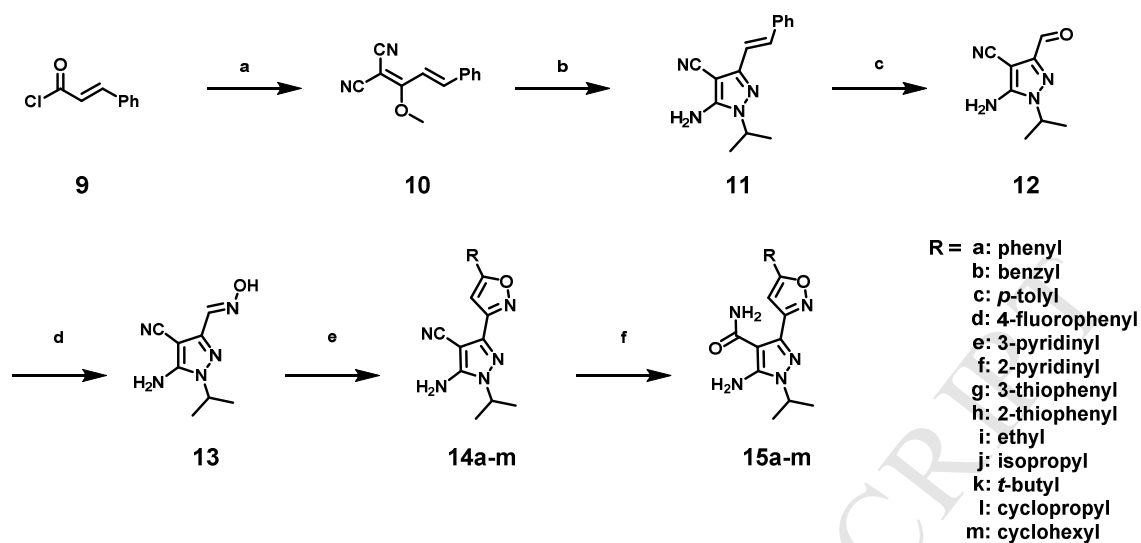


Scheme 1. Synthesis of inhibitor **8**^a

^aReagent and condition: (a) 4 N HCl in dioxane, EtOH, rt, 90%; (b) DL-serine methyl ester hydrochloride, triethylamine, CH₂Cl₂, 0 °C to rt, 73%; (c) CuBr₂, DBU, HMTA, CH₂Cl₂, 0 °C to rt, 50%; (d) i) NaOH, MeOH/H₂O, rt; ii) oxalyl chloride, *cat.*DMF, CH₂Cl₂, rt; iii) malononitrile, DIPEA, THF, 0 °C to rt; iv) dimethylsulfate, THF, reflux; (e) isopropylhydrazine hydrochloride, triethylamine, EtOH, rt; (f) formamide, 160 °C, 26% over 3 steps.

Guided by this reasoning, we prepared 3-(2-cyclopropyloxazol-4-yl)-1-isopropyl-1*H*-pyrazolo[3,4-*d*]pyrimidin-4-amine (**8**) starting with commercially available cyclopropyl cyanide employing the route displayed in Scheme 1. Ethanol addition to **1** under acidic conditions led to ethyl cyclopropanecarbimide (**2**) as a hydrochloride salt, which was condensed with DL-serine methyl ester to give oxazoline **3** [27]. Subsequent oxidation of **3** with cupric bromide afforded oxazole **4** [28], which was transformed to the target **8** using a previously described procedure [18]. Both the *in vitro* inhibitory activity of **8** against RET and its metabolic stability in mouse liver microsomes were evaluated. Unfortunately, this oxazole derivative was found to display moderate RET inhibitory activity (IC₅₀ = 0.139 μM) and it does not have an improved microsomal stability (2.8% remaining during 15 min) compared to **6g** (Table 1).

These findings suggested that, even though it has been widely applied in several types of drugs, the pyrazolo[3,4-*d*]pyrimidine moiety in **6g** is the likely source of its poor metabolic stability. We noted that 5-aminopyrazole-4-carboxamide group could act as a replacement for the pyrazolo[3,4-*d*]pyrimidine ring system in drugs [29]. We also reasoned that the 5-aminopyrazole-4-carboxamide group might serve as an effective substitute because intramolecular hydrogen bonding between the 5-amine and 4-carboxamide groups might enable it to possess the same bioactive conformation as that in the flat fused pyrazolo[3,4-*d*]pyrimidine ring system (Figure 1B).



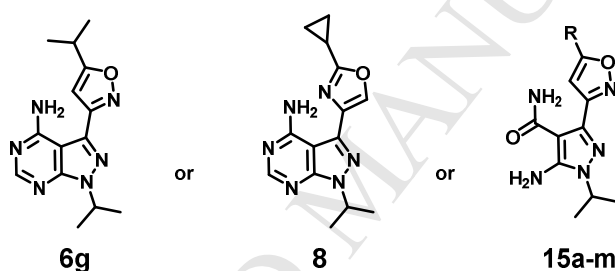
Scheme 2. Synthesis of inhibitors **15a-m**^a

^aReagent and condition: (a) i) malononitrile, DIPEA, THF, 0 °C to rt; ii) dimethylsulfate, THF, reflux, 79%; (b) isopropyl hydrazine hydrochloride, triethylamine, EtOH, 0 °C to rt, 82%; (c) i) OsO₄, NMO, THF/H₂O, 0 °C to rt; ii) NaIO₄, THF/H₂O, 0 °C to rt; (d) hydroxylamine hydrochloride, NaOAc, EtOH, rt, 71%; (e) various acetylenes, NaOCl, dioxane, 0 °C to rt; (f) acetaloxime, PPh₃, Pd(OAc)₂, EtOH/ H₂O, 100 °C, 15-35% over 2 steps.

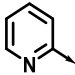
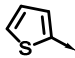
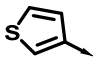

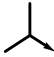


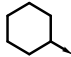
In order to explore this hypothesis, we prepared and determined the RET kinase inhibitory activities of the 5-aminopyrazole-4-carboxamide derivatives **15a-m** (Scheme 2). We fixed the functional group attached to the pyrazole ring as an isopropyl group as it has already been optimized in our previous study [18]. The synthesis of these substances commenced with sequential transformation of cinnamoyl chloride (**9**) to the bis-nitrile **10** and pyrazole **11**. Dihydroxylation of **11** and subsequent oxidative cleavage produced the corresponding aldehyde **12**, which was condensed with hydroxylamine to afford the key oxime intermediate **13**. In a first attempt to prepare the targets, the nitrile group in **13** was hydrolyzed to generate the corresponding carboxamide, which was then subjected to the nitrile-oxide cycloaddition (NOC) reaction using several oxidizing agents, such as NaOCl, *t*-BuOCl and phenyliodine-bis(trifluoroacetate) (PIFA) in the presence of acetylenes. None of

these reactions resulted in production of the desired isoxazoles. As a result, the synthetic sequence was changed so that the nitrile-oxide cycloaddition (NOC) reaction was carried out prior to nitrile hydrolysis. Among the oxidizing reagents described above, NaOCl successfully converted **13** to the nitrile oxide that underwent cycloaddition with selected acetylenes to form **14a-m**. Hydrolysis of nitrile group in these substances, accomplished using Pd(OAc)₂ and PPh₃, generated the targets **15a-m** [30].

Table 1. Results of *in vitro* biochemical kinase assays for inhibition of RET kinase and microsomal stabilities of **8** and **15a-m**.



Compound	R	RET IC ₅₀ (μM) ^a	Microsomal stability (% remaining) ^b
6g	-	0.041	5.10
8	-	0.139	2.80
15a		0.236	60.8
15b		1.639	54.6
15c		1.661	61.8
15d		0.416	85.2
15e		3.395	86.7

15f		4.803	49.0
15g		0.078	32.1
15h		0.162	11.8
15i		0.631	15.1
15j		1.259	51.6
15k		2.224	78.0
15l		0.044	62.5
15m		2.695	40.6

^aA radiometric biochemical kinase assay. ^bMouse liver microsomal stability after 1 μM treatment for 15 min.

The RET kinase inhibitory activities and mouse microsomal stabilities of the 5-aminopyrazole-4-carboxamides **15a-m** were determined. Interestingly, these substances were found to have highly enhanced microsomal stabilities compared to that of **6g**. In particular, **15j** showed a 10-fold greater microsomal stability than **6g** even though both substances contain an isopropyl group. This observation indicates that the 5-aminopyrazole-4-carboxamide scaffold is a critical factor governing metabolic stability. The RET kinase inhibitory activities (IC_{50}) of **15a-m**, were found to be in the range of 0.044-4.803 μM , suggesting that the nature of the isoxazole R group, which occupies a highly hydrophobic back pocket [31] of the RET kinase, governs the degree of inhibition. The phenyl group in **15a** leads to a moderate level of inhibition ($\text{IC}_{50} = 0.236 \mu\text{M}$) whereas the benzyl group **15b** causes a 7-fold decrease in activity ($\text{IC}_{50} = 1.639 \mu\text{M}$). Methyl substitution at the *para*-position of the phenyl ring (**15c**) also reduces the inhibitory activity ($\text{IC}_{50} = 1.661 \mu\text{M}$). However, replacement of *para*-methyl in **15c** with electron-withdrawing substituents such as *p*-fluoro (**15d**) gives rise to a moderate inhibition potency ($\text{IC}_{50} = 0.416 \mu\text{M}$). The effects of several heteroaromatic isoxazole

substituents were explored. The results show that the inhibitory activities of pyridine-containing analogues **15e**, **15f** are much lower ($IC_{50} = 3.395 \mu\text{M}$ and $4.803 \mu\text{M}$, respectively), which indicates the existence of a hydrophobic pocket in the RET kinase binding site. Unlike pyridine, the thiophene group in **15g** and **15h**, which has an electronic character that is similar to that of benzene, causes an increase in activity ($IC_{50} = 0.078 \mu\text{M}$ and $0.162 \mu\text{M}$, respectively). Incorporation of alkyl substituents in the isoxazole ring leads to a size dependent effect on inhibition (ethyl, **15i**, $IC_{50} = 0.631 \mu\text{M}$, isopropyl, **15j**, $IC_{50} = 1.259 \mu\text{M}$, and *t*-butyl, **15k**, $IC_{50} = 2.224 \mu\text{M}$). Likewise, carbocyclic groups also display a size-dependent effect on inhibitory activity. Finally, the substance possessing a cyclopropyl group (**15l**) has a high potency ($IC_{50} = 0.044 \mu\text{M}$), but the analogue with a bulky cyclohexyl group (**15m**) has low inhibitory activity ($IC_{50} = 2.695 \mu\text{M}$). The combined results show that **15l** has an optimal RET kinase inhibitory activity and high microsomal stability (62.5% remaining after 15 min) in mouse liver microsomes. In further metabolic stability study, **15l** exhibited significantly enhanced metabolic stability in rat and human liver microsomes compared with **6g** (Supplementary Table 1).

Based on the promising results summarized above, we investigated the biological properties of the three most potent wild-type RET inhibitors **15g**, **15h** and **15l**. First, the inhibitory activities of these substances against RET-V804M, the clinically identified gatekeeper mutation that is resistant to cabozantinib and whose bulkier methionine residue impedes inhibitor binding, were determined. All three compounds were observed to have a lower activity against this mutant than they have against wild-type RET. Among the three, **15l** that has the highest inhibitory activity against wild-type RET also potently inhibits RET-V804M with an IC_{50} value of $0.252 \mu\text{M}$. This is a remarkable finding considering the inhibitory activity of clinically-approved cabozantinib against RET-V804M ($IC_{50} = 0.358 \mu\text{M}$). We also assessed the cellular activities of **15g**, **15h** and **15l** using RET-transformed Ba/F3 cells and the two human-driven thyroid cells, TT and Nthy ori-3-1. TT cells are MTC cells harboring the RET-C634W mutation and Nthy ori-3-1 cells are normal thyroid cells that are used to monitor the differential cytotoxicity of RET inhibitors. In contrast to expectations, **15g** and **15h** containing a thiophene group do not display anti-proliferative activities on RET Ba/F3 cells as well as

the other two cell lines. This result indicates that the potent RET inhibitory activities of these substances observed in a biochemical kinase assay are not reflected in cellular potency. However, **15l** which has the highest potency against both wild-type RET and RET-V804M not only effectively inhibits wild-type RET and RET-V804M transformed Ba/F3 cells ($GI_{50} = 0.87 \mu\text{M}$ and $6.98 \mu\text{M}$, respectively), but it also suppresses growth of TT cells ($GI_{50} = 1.66 \mu\text{M}$) without having an influence on parental Ba/F3 and Nthy ori-3-1 cells ($GI_{50} > 10 \mu\text{M}$) which is normal thyroid cells. In comparison to the effects of cabozantinib, **15l** has a slightly lower potency against all three cells. However, the activities of **15l** are noteworthy considering its exceptional kinase selectivity (see below) and the multi-targeted characteristics of cabozantinib and its significant level of growth inhibition on even Nthy ori-3-1 cells ($GI_{50} = 2.92 \mu\text{M}$).

Table 2. Inhibitory activities of **15g**, **15h** and **15l** against RET, RET-V804M and thyroid cell lines.

Compound	Enzyme assays (IC_{50} , μM) ^a		Cell assays (GI_{50} , μM)				
	RET	RET-V804M	Ba/F3 cells		Thyroid cells		
			Parental	RET	RET-V804M	TT	Nthy ori-3-1
15g	0.078	1.218	>10	>10	>10	>10	>10
15h	0.162	2.902	>10	>10	>10	>10	>10
15l	0.044	0.252	>10	0.87 ± 0.16	6.98 ± 1.38	1.66 ± 0.10	>10
cabozantinib	0.009^b	0.358^b	>10	0.07 ± 0.01	0.74 ± 0.05	0.26 ± 0.11	2.92 ± 0.57

^aRadiometric biochemical kinase assay. ^bPublished results [18]

To better understand the RET-WT and RET-V804M inhibitory activities of 5-aminopyrazole-4-carboxamides, we performed molecular docking study of **15l** based upon the crystal structure of RET

kinase (PDB accession code: 2IVV) using Schrödinger docking program, Glide (Figure 2). Analysis of the predicted binding mode shows that as expected, the carbonyl group of the 4-carboxamide moiety forms an intramolecular hydrogen bond with the 5-amine group on the pyrazole ring, which helps to stabilize a planar conformation. The fixed orientation of carboxamide moiety enables it to form hydrogen bonds with both Glu805 and Ala807 in the hinge region, which is the same as that occurs with the bioactive conformation of pyrazolo[3,4-*d*]pyrimidines [18]. Also, the cyclopropyl group of **151** occupies a hydrophobic back pocket in the ATP binding site, and the oxygen and nitrogen of isoxazole ring form hydrogen bonds with the ammonium group of Lys758 and hydroxyl group of Ser891, respectively (Figure 2A, 2B). As a consequence of these hydrogen bonds at the hinge region and with Lys758 and Ser891, along with the hydrophobic interaction provided by the cyclopropyl group, **151** is predicted to be a tight binding inhibitor at the ATP binding site of RET kinase. In addition, the relatively small cyclopropyl group would be sterically less affected by the sterically more crowded gatekeeper region in the V804M mutant (see Figure 2 B'').

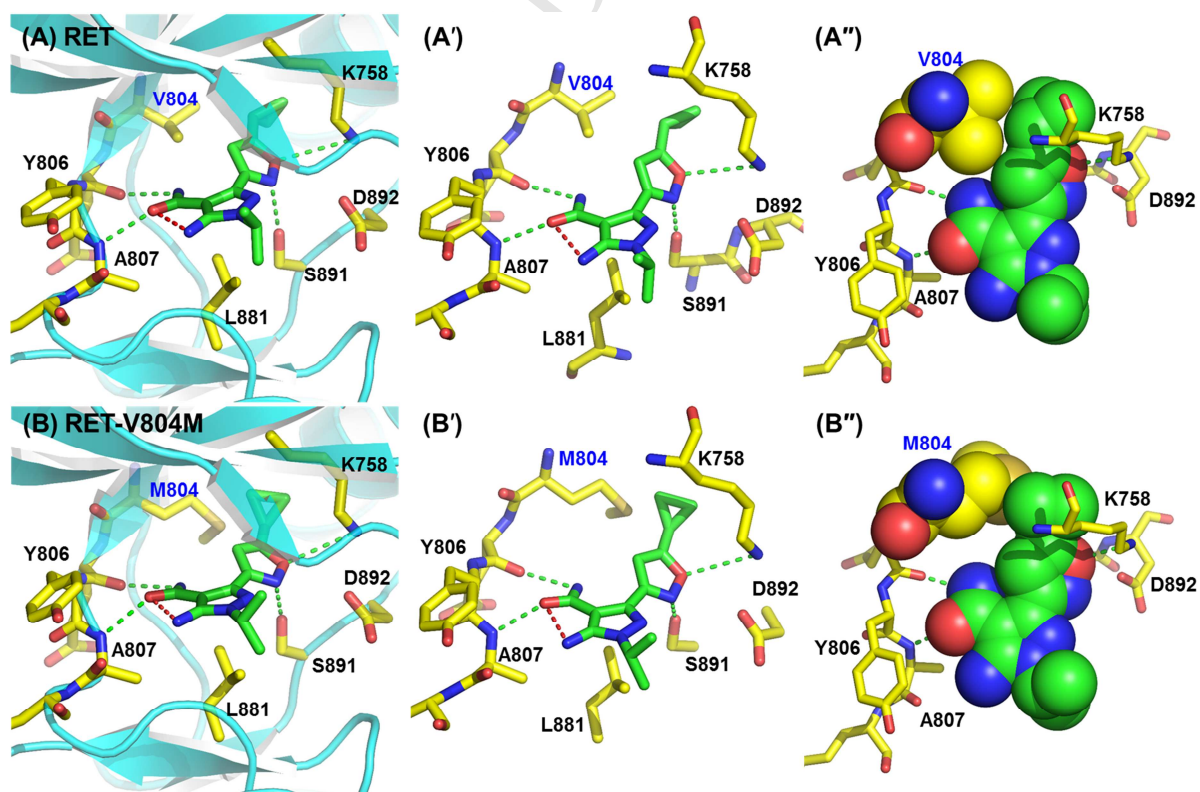


Figure 2. Calculated binding model of **15l** complexed to (A) wild-type RET and (B) gatekeeper mutant (V804M) of RET kinase. Dashed green lines denote hydrogen bonding interactions. Dashed red line denotes an intramolecular hydrogen bond in **15l** compound. (A', B') Crucial residues for the interaction of **15l** with RET kinase domain. (A'', B'') Space-filling model which reflects electronic surfaces for V804 (or M804) and **15l** compound.

In order to evaluate the kinase selectivity of **15l**, kinome-wide selectivity profiling was carried out using a panel of 369 kinases at a concentration of 1 μ M. Surprisingly, the profiling results demonstrate that **15l** does not cause a greater than 90% inhibition ($S_{10} = 0.01$) of any kinases other than RET. This outstanding RET selectivity is meaningful in terms of both medicinal chemistry and chemical biology, because it suggests that **15l** should not only serve as a lead compound to develop highly selective cancer therapeutics, but it should also be an excellent chemical probe to explore RET-related biological pathways.

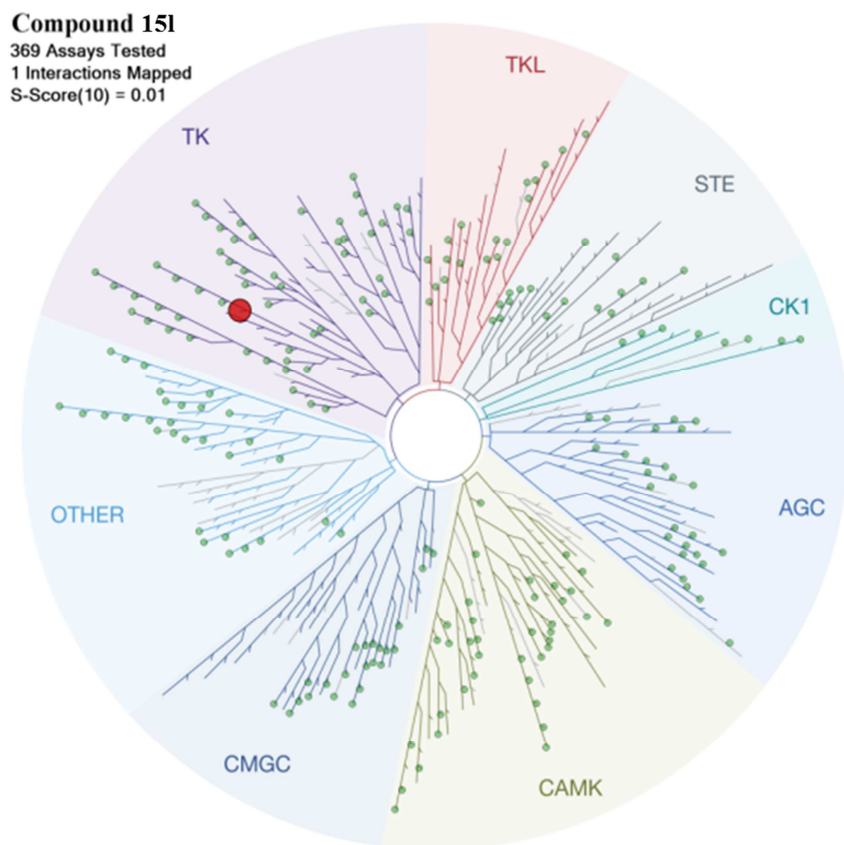


Figure 3. Kinome-wide selectivity profiling of **151** at 1 μ M with a cutoff of 90% inhibition.

To determine if **151** is capable of decreasing the level of RET phosphorylation and deactivating downstream molecules in a cellular context, western blot analysis was performed using Ba/F3 cells transformed with RET-V804M gatekeeper mutant as well as wild-type RET. In agreement with the results of the *in vitro* biochemical kinase assays and Ba/F3 cellular assays, **151** effectively attenuates autophosphorylation of RET at Y905 and Y1062 and its adaptor proteins such as PLC γ and Shc in a dose dependent manner (Figure 4). We also determined whether **151** can induce apoptosis of wild-type RET and RET-V804M Ba/F3 cells. This analysis revealed that the level of cleaved PARP is elevated in **151** treated wild-type RET Ba/F3 and RET-V804M Ba/F3 cells (Figure 5A, B), but not in **151** treated normal thyroid Nthy ori-3-1 cells (Figure 5C). The results demonstrate that the anti-proliferative activity of **151** is associated with its apoptosis induction capability. It is noteworthy that

cabozantinib induces apoptosis in the Nthy ori-3-1, normal thyroid cells while **15I** does not even at a concentration of 20 μM . In the final phase of this study, we assessed the effect of **15I** on anchorage independent growth, which is a hallmark of cancer cells. As can be seen by viewing the profiles in Figure 6, obtained employing a soft agar assay conducted over a 4 w period with TT thyroid cancer cells, the size and number of colonies are significantly diminished as the concentration of **15I** increases. This finding demonstrates that this substance is capable of suppressing the anchorage independent growth of TT thyroid cancer cells.

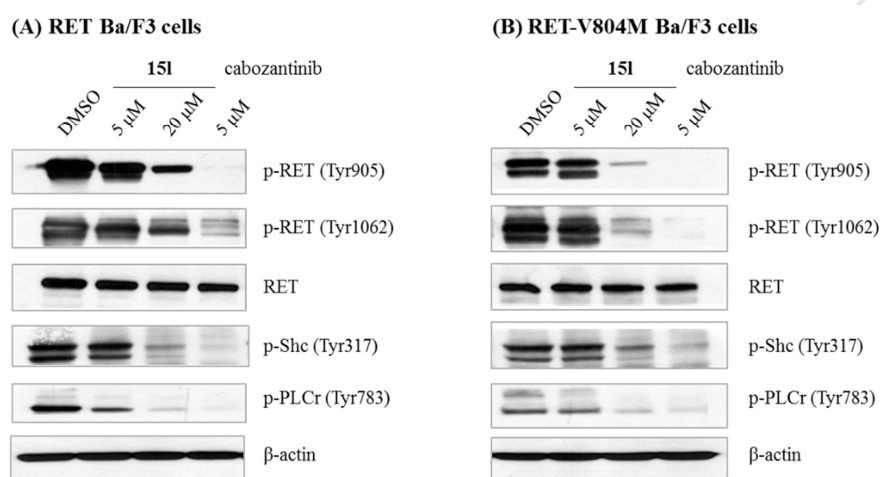


Figure 4. Autophosphorylation of RET and its downstream signaling are blocked by **15I**. (A) RET-Ba/F3 cells. (B) RET-V804M Ba/F3 cells. RET and RET-V804M Ba/F3 cell lines were treated with **15I** (5 μM , 20 μM) and cabozantinib (5 μM) for 3 h. The levels of phosphorylation of RET and its downstream targets were analyzed by western blotting.

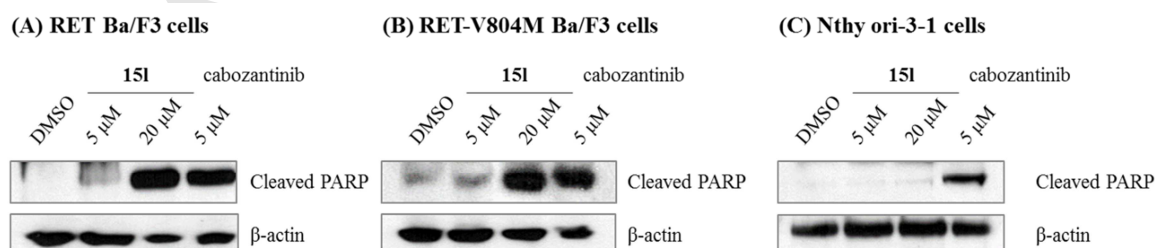


Figure 5. Compound **15I** induces apoptosis in (A) RET-Ba/F3 cells, (B) RET-V804M Ba/F3 cells but

not in (C) Nthy ori-3-1 cells. The cells were treated with **15I** (5 μ M, 20 μ M) and cabozantinib (5 μ M) for 48 h. Whole lysates were immunoblotted with the indicated antibodies.

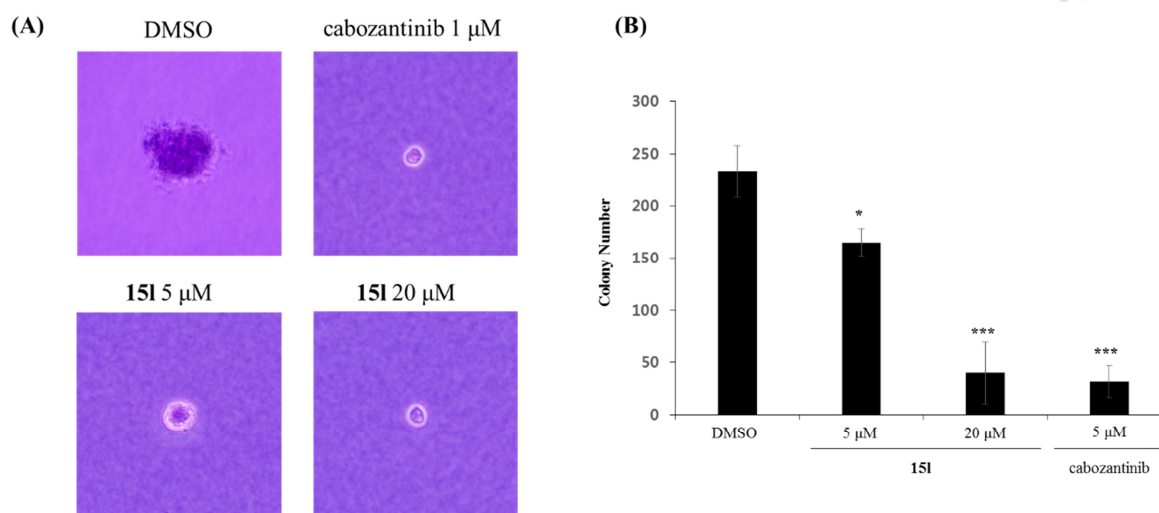


Figure 6. Anchorage independent growth of TT cells is suppressed by treatment with **15I**. (A) Effects of **15I** and cabozantinib on anchorage independent growth of TT cell in soft agar. For measurement of the colony forming ability, TT cells were plated in 6 well plate and then treated with **15I** and cabozantinib for 4 w. Colonies were fixed and stained with 0.005% crystal violet ($n = 3$) and (B) counted by using Image J software program. The data are presented with \pm S.D of data from three independent experiments performed in triplicate. *t*-test * $P < 0.05$, *** $P < 0.005$.

3. Conclusions

The investigation described above was designed to find the site in the RET kinase inhibitor **6g** that leads to its metabolic instability. The working hypothesis was that the poor stability of this substance is associated with the isoxazole moiety, which is known to be a readily cleaved 5-membered heterocycle. Differing from this expectation, we observed that replacement of the isoxazole group by the more stable oxazole has no effect on metabolic stability. The finding suggested that, although

known to be a biologically stable scaffold, the pyrazolo[3,4-*d*]pyrimidine moiety is responsible for the instability of **6g**. We reasoned that because of an intramolecular hydrogen bonding interaction, the 5-aminopyrazole-4-carboxamide group would possess the same bioactive conformation as does the flat fused pyrazolo[3,4-*d*]pyrimidine ring system. Interestingly, isoxazole containing 5-aminopyrazole-4-carboxamide derivative were found to have highly improved microsomal stabilities and retained RET kinase inhibitory activities. A comprehensive SAR study led to the observation that **15l** possesses a high potency against RET-V804M as well as against wild-type RET in both enzymatic and cellular assays. This substance also displays an exceptional kinase selectivity in that RET is the only kinase among 369 that it inhibits. Owing to its outstanding specificity, excellent potency and improved microsomal stability, **15l** should be a key tool in studies aimed at understanding RET biology. Finally, the strategy employed in this effort, involving the use of bioisosteric replacement of pyrazolo[3,4-*d*]pyrimidine by a 5-aminopyrazole-4-carboxamide group has potential applications in other drug discovery programs.

4. Experimental

4.1. Chemistry

Unless otherwise described, all commercial reagents and solvents were purchased from commercial suppliers and used without further purification. All reactions were performed under N₂ atmosphere in flame-dried glassware. Reactions were monitored by TLC with 0.25 mm E. Merck precoated silica gel plates (60 F254). All solvents were purified by standard techniques. Purification of reaction products was carried out by silica gel column chromatography using Kieselgel 60 Art. 9385 (230–400 mesh). The purity of all compounds was over 95%, and mass spectra and purity of all compounds was analyzed using Waters LCMS system (Waters 2998 Photodiode Array Detector, Waters 3100 Mass Detector, Waters SFO System Fluidics Organizer, Water 2545 Binary Gradient Module, Waters Reagent Manager, Waters 2767 Sample Manager) using SunFire™ C18 column (4.6 × 50 mm, 5 μm

particle size): solvent gradient = 60% (or 95%) A at 0 min, 1% A at 5 min. Solvent A = 0.035% TFA in H₂O; Solvent B = 0.035% TFA in MeOH; flow rate 3.0 (or 2.5) mL/min. ¹H and ¹³C NMR spectra were obtained using a Bruker 400 MHz FT-NMR (400 MHz for ¹H, and 100 MHz for ¹³C) spectrometer. Standard abbreviations are used for denoting the signal multiplicities.

4.1.1. Ethyl cyclopropanecarbimide hydrochloride (2). To a solution of cyclopropyl cyanide (7.45 mL, 100 mmol) in EtOH (6.13 mL) was added 4 N HCl in dioxane (75 mL) at room temperature. The reaction mixture was then stirred for 12 h at room temperature, solidified by adding diethyl ether. The resulting solid was filtered to afford **2** (13.53 g, 90%) as a white solid. ¹H NMR (400 MHz, CD₃OD) δ 4.38 (q, *J* = 6.8 Hz, 2H), 3.30 (pent, *J* = 1.6 Hz, 1H), 1.41 (t, *J* = 7.2 Hz, 3H), 1.30-1.28 (m, 4H).

4.1.2. Methyl 2-cyclopropyl-4,5-dihydrooxazole-4-carboxylate (3). To a solution of **2** (13.53 g, 90.4 mmol) and DL-serine methyl ester (15 g, 94.9 mmol) in CH₂Cl₂ (100 mL) was added trimethylamine (28 mL, 199 mmol) at 0 °C. The reaction mixture was allowed to warm to room temperature and stirred for 12 h. The reaction mixture was diluted with CH₂Cl₂, quenched with H₂O. The organic layer was washed with H₂O, and dried over MgSO₄, filtered, and concentrated under reduced pressure. The residue was purified by flash column chromatography on silica gel (50% EtOAc/hexane) to afford **3** (11.16 g, 73%) as a yellow liquid. ¹H NMR (400 MHz, CDCl₃) δ 4.69 (dd, *J* = 7.6 Hz, 10.4 Hz, 1H), 4.46-4.42 (m, 1H), 4.35 (dd, *J* = 8.4 Hz, 10.4 Hz, 1H), 3.78 (s, 3H), 1.74-1.61 (m, 1H), 1.01-0.97 (m, 2H), 0.90-0.85 (m, 2H).

4.1.3. Methyl 2-cyclopropyloxazole-4-carboxylate (4). To a solution of CuBr₂ (2.8 g, 12.54 mmol) in CH₂Cl₂ (18 mL) was added hexamethylenetetramine (HMTA, 1.76 g, 12.54 mmol) and DBU (1.9 mL, 12.54 mmol) sequentially at 0 °C. After 20 min, the reaction mixture was treated with a solution of **3** (850 mg, 5.01 mmol) in CH₂Cl₂ (6 mL) at 0 °C and was allowed to warm to room temperature and stirred for 3 h. The reaction mixture was diluted with CH₂Cl₂, quenched with H₂O. The organic layer was washed with H₂O, and dried over MgSO₄, filtered, and concentrated under reduced pressure. The residue was purified by flash column chromatography on silica gel (40% EtOAc/hexane) to afford **4** (419 mg, 50%) as a colorless oil. ¹H NMR (400 MHz, CDCl₃) δ 8.07 (s, 1H), 3.89 (s, 3H), 2.14-2.07

(m, 1H), 1.17-1.11 (m, 2H), 1.10-1.05 (m, 2H); ^{13}C NMR (100 MHz, CDCl_3) δ 167.12, 161.82, 142.97, 133.17, 52.08, 8.83, 8.53.

4.1.4. 3-(2-cyclopropyloxazol-4-yl)-1-isopropyl-1H-pyrazolo[3,4-d]pyrimidin-4-amine (8). To a solution of **4** (407 mg, 2.43 mmol) in EtOH (5 mL) was added sodium hydroxide (970 mg, 24.3 mmol) at room temperature. The reaction mixture was stirred for 2 h, diluted with EtOAc, and quenched with 1 N HCl for adjusting the pH to 2 and then extracted with EtOAc. The organic layer was washed with H_2O , dried over MgSO_4 , filtered, and concentrated under reduced pressure to afford crude acid **5**. To a solution of resulting acid **5** in CH_2Cl_2 (12 mL) was added oxalyl chloride (0.48 mL, 5.65 mmol) and DMF (0.02 mL). The reaction mixture was stirred for 2 h and concentrated under reduced pressure. The resulting solid was diluted with THF (8 mL) and treated with malononitrile (180 mg, 2.71 mmol). The reaction mixture was cooled to 0 °C, treated slowly with DIPEA (0.98 mL, 5.65 mmol), and then allowed to warm to room temperature and stirred for 2 h. Afterward, the reaction mixture was treated with dimethyl sulfate (0.64 mL, 6.78 mmol) and then stirred for 6 h at 70 °C. The mixture was cooled to room temperature and quenched with H_2O . The aqueous layer was extracted with EtOAc. The combined organic layers were dried over MgSO_4 , filtered, and concentrated under reduced pressure. The residue was roughly purified by flash column chromatography on silica gel (33% EtOAc/hexane) to afford **5** as a yellow oil with some other side products. The resulting oil was diluted with EtOH (7 mL), treated with isopropyl hydrazine hydrochloride (173 mg, 1.57 mmol) and triethylamine at room temperature. The reaction mixture was stirred for 30 min and diluted with EtOAc. The organic layer was washed with H_2O , dried over MgSO_4 , filtered, and concentrated under reduced pressure. The resulting crude product was used for the next step without further purification. The resulting pyrazole **6** was dissolved in formamide (1.2 mL). The reaction mixture was stirred for 16 h at 160 °C and then cooled to room temperature. The mixture was cooled to room temperature and quenched with H_2O . The aqueous layer was extracted with EtOAc. The combined organic layers were dried over MgSO_4 , filtered, and concentrated under reduced pressure. The residue was purified by flash column chromatography on silica gel (50% EtOAc/hexane) to afford **8** (180 mg, 26% over 3 steps) as a white solid. ^1H NMR (400 MHz, CDCl_3) δ 9.46 (bs, 1H), 8.30 (s, 1H), 8.07 (s, 1H), 5.95 (bs, 1H), 5.12 (sep,

$J = 6.8$ Hz, 1H), 2.18-2.11 (m, 1H), 1.54 (d, $J = 6.4$ Hz, 6H), 1.13-1.11 (m, 4H); ^{13}C NMR (100 MHz, CDCl_3) δ 166.25, 158.26, 155.58, 153.21, 135.90, 134.47, 134.23, 98.57, 48.86, 21.96, 8.98, 8.59. LCMS (ESI) m/z : 285 $[\text{M}+\text{H}]^+$.

4.1.5. (*E*)-2-(1-Methoxy-3-phenylallylidene)malononitrile (**10**). To a solution of cinnamoyl chloride (5 g, 30.0 mmol) in dry THF (100 mL) was added malononitrile (2.38 g, 36.0 mmol) and diisopropylethylamine (13.1 mL, 75.03 mmol) at 0 °C. The reaction mixture was then stirred for 1 h at room temperature. After adding the dimethylsulfate (8.6 mL, 80 mmol) at room temperature, the reaction mixture was refluxed for 12 h. The reaction mixture was diluted with EtOAc. The organic layer was washed with H_2O , and dried over MgSO_4 , filtered, and concentrated under reduced pressure. The residue was purified by flash column chromatography on silica gel (10% EtOAc/hexane) to afford **10** (4.99 g, 79%) as a yellow solid. ^1H NMR (400 MHz, CDCl_3) δ 7.58-7.54 (m, 3H), 7.46-7.39 (m, 3H), 6.96 (d, $J = 15.6$ Hz, 1H), 4.35 (s, 3H); ^{13}C NMR (100 MHz, CDCl_3) δ 177.97, 144.25, 133.46, 131.40, 129.06, 128.51, 117.07, 113.66, 112.96, 77.31, 76.99, 76.67, 63.80, 61.01.

4.1.6. (*E*)-5-Amino-1-isopropyl-3-styryl-1H-pyrazole-4-carbonitrile (**11**). To a solution of **10** (4.3 g, 20.5 mmol) in MeOH (110 mL) was added isopropyl hydrazine hydrochloride (3.4 g, 30.8 mmol) and trimethylamine (11.4 mL, 82.1 mmol) at 0 °C. The reaction mixture was stirred for 1 h at room temperature and then diluted with EtOAc. The organic layer was washed with H_2O , and dried over MgSO_4 , filtered, and concentrated under reduced pressure. The residue was purified by flash column chromatography on silica gel (25% EtOAc/hexane) to afford **11** (4.2 g, 82%) as a solid. ^1H NMR (400 MHz, CDCl_3) δ 7.52-7.50 (m, 2H), 7.44 (d, $J = 16.8$ Hz, 1H), 7.35-7.32 (m, 2H), 7.27 (d, $J = 7.6$ Hz, 1H), 6.98 (d, $J = 16.8$ Hz, 1H), 4.20 (bs, 2H), 4.20 (pen, $J = 6.4$ Hz, 1H), 1.48 (d, $J = 6.4$ Hz, 6H).

4.1.7. (*E*)-5-Amino-3-((hydroxyimino)methyl)-1-isopropyl-4,5-dihydro-1H-pyrazole-4-carbonitrile (**13**). To a solution of **11** (4.2 g, 16.7 mmol) in THF/ H_2O (3:1, 225 mL) was added 4-methylmorpholine *N*-oxide (50% solution in H_2O , 33.4 mmol, 10.7 mL) and OsO_4 (4% solution in H_2O , 10.7 mL, 1.67 mmol) at 0 °C. The reaction mixture was allowed to warm to room temperature and stirred for 10 h. The reaction was quenched with saturated Na_2SO_3 solution and extracted with mixed solution of CHCl_3 /IPA (4:1). The organic phase was washed with water, and dried over MgSO_4

and concentrated under reduced pressure to afford crude diol. To a solution of the resulting diol in THF/H₂O (3:1, 225 mL), was added NaIO₄ (10.7 g, 50.1 mmol) at room temperature. The reaction mixture was stirred for 2 h at room temperature. The suspended mixture was filtered through celite pad and extracted with EtOAc. The organic phase was washed with water and brine, dried over MgSO₄, and concentrated under reduced pressure to afford the crude aldehyde **12**. To a solution of the crude aldehyde **12** in EtOH (100 mL) was added hydroxylamine hydrochloride (2.9 g, 41.8 mmol) and NaOAc (3.3 g, 40.08 mmol) at room temperature. The reaction mixture was stirred for 3 h and concentrated under reduced pressure. The residue was purified by flash column chromatography on silica gel (50% EtOAc/hexane) to afford oxime **13** (2.3 g, 71%) as a white solid. ¹H NMR (400 MHz, DMSO) δ 11.52 (s, 1H), 7.86 (s, 1H), 6.64 (bs, 2H), 4.45 (pent, *J* = 6.4 Hz, 1H), 1.27 (d, *J* = 6.4 Hz, 6H).

4.1.8. General Procedure A for the Synthesis of Compounds 15a-m. To a solution of **13** (1 equiv) and various acetylene (1.2 equiv) in dioxane (0.1M) was added NaOCl (14% available chlorine liquid, 1 mL/mmol) at room temperature. The reaction mixture was stirred for 1 h at room temperature, quenched with H₂O, and diluted with EtOAc. The organic layer was washed with water and brine, dried over MgSO₄, filtered and concentrated under reduced pressure. And then, to a solution of crude compound in EtOH/H₂O (4:1, 0.2M) was added Pd(OAc)₂ (0.1 equiv), PPh₃ (0.2 equiv) and acetaloxime (2 equiv) at room temperature. The reaction mixture was stirred for 1 h at 100 °C, filtered through celite pad, and extracted with EtOAc. The organic phase was washed with water and brine, dried over MgSO₄, and concentrated under reduced pressure. The residue was purified by flash column chromatography on silica gel.

4.1.8.1. 5-Amino-1-isopropyl-3-(5-phenylisoxazol-3-yl)-1H-pyrazole-4-carboxamide (15a).

Compound **13** (200 mg, 1.0 mmol) was converted to the target compound using general procedure A. The crude product was purified by flash column chromatography on silica gel (35% EtOAc/hexane to 70% EtOAc/hexane) to afford **15a** (69 mg, 22% over 2 steps) as a solid. ¹H NMR (400 MHz, CDCl₃) δ 9.42 (bs, 1H), 7.85-7.83 (m, 2H), 7.51-7.46 (m, 3H), 7.08 (s, 1H), 5.63 (bs, 1H), 4.33-4.26 (m, 1H), 1.52(d, *J* = 6.8 Hz, 6H); ¹³C NMR (100 MHz, CDCl₃) δ 169.04, 166.95, 159.36, 150.72, 136.56,

130.46, 129.06, 127.04, 125.97, 99.23, 95.65, 48.75, 21.42. LCMS (ESI) m/z : 312 $[M+H]^+$.

4.1.8.2. *5-Amino-3-(5-benzylisoxazol-3-yl)-1-isopropyl-1H-pyrazole-4-carboxamide* (**15b**).

Compound **13** (200 mg, 1.0 mmol) was converted to the target compound using general procedure A. The crude product was purified by flash column chromatography on silica gel (35% EtOAc/hexane to 70% EtOAc/hexane) to afford **15b** (75 mg, 23% over 2 steps) as a solid. ^1H NMR (400 MHz, CDCl_3) δ 9.42 (bs, 1H), 7.38-7.26 (m, 5H), 6.50 (s, 1H), 5.64 (bs, 1H), 4.30-4.20 (m, 1H), 4.12 (s, 2H), 1.46 (d, $J = 6.4$ Hz, 6H); ^{13}C NMR (100 MHz, CDCl_3) δ 171.20, 166.99, 158.90, 150.68, 136.59, 135.62, 128.91, 128.88, 127.26, 101.67, 95.52, 48.66, 33.02, 21.36. LCMS (ESI) m/z : 326 $[M+H]^+$.

4.1.8.3. *5-Amino-1-isopropyl-3-(5-(p-tolyl)isoxazol-3-yl)-1H-pyrazole-4-carboxamide* (**15c**).

Compound **13** (200 mg, 1.0 mmol) was converted to the target compound using general procedure A. The crude product was purified by flash column chromatography on silica gel (35% EtOAc/hexane to 70% EtOAc/hexane) to afford **15c** (84 mg, 26% over 2 steps) as a solid. ^1H NMR (400 MHz, CDCl_3) δ 9.34 (bs, 1H), 7.73 (d, $J = 8.0$ Hz, 2H), 7.28 (t, $J = 8.0$ Hz, 2H), 7.02 (s, 1H), 5.72 (bs, 2H), 5.45 (bs, 1H), 4.30 (sep, $J = 6.4$ Hz, 1H), 2.42 (s, 3H), 1.52 (d, $J = 6.4$ Hz, 6H); ^{13}C NMR (100 MHz, CDCl_3) δ 169.26, 166.86, 159.36, 150.71, 140.70, 136.64, 129.66, 125.89, 124.44, 98.62, 95.83, 48.76, 21.38, 21.31. LCMS (ESI) m/z : 326 $[M+H]^+$.

4.1.8.4. *5-Amino-3-(5-(4-fluorophenyl)isoxazol-3-yl)-1-isopropyl-1H-pyrazole-4-carboxamide* (**15d**).

Compound **13** (200 mg, 1.0 mmol) was converted to the target compound using general procedure A. The crude product was purified by flash column chromatography on silica gel (35% EtOAc/hexane to 70% EtOAc/hexane) to afford **15d** (63 mg, 19% over 2 steps) as a solid. ^1H NMR (400 MHz, CDCl_3) δ 9.32 (bs, 1H), 7.85-7.81 (s, 2H), 7.21-7.16 (m, 2H), 7.03 (s, 1H), 5.56 (bs, 1H), 4.30 (sep, $J = 6.8$ Hz, 1H), 1.52 (d, $J = 6.8$ Hz, 6H); ^{13}C NMR (100 MHz, CDCl_3) δ 168.06, 166.82, 165.18, 162.68, 159.47, 150.72, 136.41, 128.09, 128.01, 123.47, 123.43, 116.40, 116.18, 99.05, 95.76, 48.76, 21.39. LCMS (ESI) m/z : 330 $[M+H]^+$.

4.1.8.5. *5-Amino-1-isopropyl-3-(5-(pyridin-3-yl)isoxazol-3-yl)-1H-pyrazole-4-carboxamide* (**15e**).

Compound **13** (200 mg, 1.0 mmol) was converted to the target compound using general procedure A. The crude product was purified by flash column chromatography on silica gel (35% EtOAc/hexane to

70% EtOAc/hexane) to afford **15e** (87 mg, 28% over 2 steps) as a solid. ^1H NMR (400 MHz, CDCl_3) δ 9.20 (bs, 1H), 9.08 (d, $J = 1.2$ Hz, 1H), 8.69 (dd, $J = 4.8$ Hz, $J = 1.6$ Hz, 1H), 8.11 (dt, $J = 8.4$ Hz, $J = 1.6$ Hz, 1H), 7.45-7.41 (m, 1H), 7.17 (s, 1H), 5.71 (bs, 2H), 5.43 (bs, 1H), 4.28 (sep, $J = 6.8$ Hz, 1H), 1.51 (d, $J = 6.8$ Hz, 6H); ^{13}C NMR (100 MHz, CDCl_3) δ 166.73, 166.16, 159.51, 151.18, 150.78, 147.17, 136.07, 132.95, 123.78, 123.31, 100.31, 95.67, 48.78, 21.37. LCMS (ESI) m/z : 313 $[\text{M}+\text{H}]^+$.

4.1.8.6. *5-Amino-1-isopropyl-3-(5-(pyridin-2-yl)isoxazol-3-yl)-1H-pyrazole-4-carboxamide (15f)*.

Compound **13** (200 mg, 1.0 mmol) was converted to the target compound using general procedure A. The crude product was purified by flash column chromatography on silica gel (35% EtOAc/hexane to 70% EtOAc/hexane) to afford **15f** (83 mg, 27% over 2 steps) as a solid. ^1H NMR (400 MHz, CDCl_3) δ 9.23 (bs, 1H), 8.72 (d, $J = 4.4$ Hz, 1H), 7.91 (d, $J = 7.6$ Hz, 1H), 7.84 (td, $J = 7.6$ Hz, $J = 2.0$ Hz, 1H), 7.47 (s, 1H), 7.38-7.35 (m, 1H), 5.70 (bs, 2H), 5.43 (bs, 1H), 4.27 (sep, $J = 6.8$ Hz, 1H), 1.49 (d, $J = 6.8$ Hz, 6H); ^{13}C NMR (100 MHz, CDCl_3) δ 168.27, 166.85, 159.81, 150.78, 150.25, 146.51, 136.95, 136.30, 124.52, 120.92, 102.30, 95.85, 48.81, 48.81, 21.35. LCMS (ESI) m/z : 313 $[\text{M}+\text{H}]^+$.

4.1.8.7. *5-Amino-1-isopropyl-3-(5-(thiophen-2-yl)isoxazol-3-yl)-1H-pyrazole-4-carboxamide (15g)*.

Compound **13** (200 mg, 1.0 mmol) was converted to the target compound using general procedure A. The crude product was purified by flash column chromatography on silica gel (35% EtOAc/hexane to 70% EtOAc/hexane) to afford **15g** (57 mg, 18% over 2 steps) as a solid. ^1H NMR (400 MHz, CDCl_3) δ 9.32 (bs, 1H), 7.56 (dd, $J = 4.0$ Hz, $J = 1.2$ Hz, 1H), 7.48 (dd, $J = 4.8$ Hz, $J = 1.2$ Hz, 1H), 7.15 (dd, $J = 4.8$ Hz, $J = 4.0$ Hz, 1H), 6.93 (s, 1H), 5.60 (bs, 1H), 4.29 (sep, $J = 6.8$ Hz, 1H), 1.51 (d, $J = 6.8$ Hz, 6H); ^{13}C NMR (100 MHz, CDCl_3) δ 164.10, 159.35, 150.70, 136.34, 128.81, 128.33, 128.12, 127.36, 98.91, 48.77, 21.38. LCMS (ESI) m/z : 318 $[\text{M}+\text{H}]^+$.

4.1.8.8. *5-Amino-1-isopropyl-3-(5-(thiophen-3-yl)isoxazol-3-yl)-1H-pyrazole-4-carboxamide (15h)*.

Compound **13** (200 mg, 1.0 mmol) was converted to the target compound using general procedure A. The crude product was purified by flash column chromatography on silica gel (35% EtOAc/hexane to 70% EtOAc/hexane) to afford **15h** (63 mg, 20% over 2 steps) as a solid. ^1H NMR (400 MHz, DMSO) δ 8.55 (bs, 2H), 8.30 (s, 1H), 7.78-7.76 (m, 1H), 7.70 (d, $J = 4.8$ Hz, 1H), 7.22 (s, 1H), 7.18 (bs, 1H), 6.80 (s, 2H), 4.58-4.52 (m, 1H), 1.37 (d, $J = 6.4$ Hz, 6H); ^{13}C NMR (100 MHz, CDCl_3) δ 165.23,

159.25, 150.68, 136.50, 128.45, 127.13, 125.43, 124.64, 98.97, 48.75, 21.39. LCMS (ESI) m/z : 318 [M+H]⁺.

4.1.8.9. *5-Amino-3-(5-ethylisoxazol-3-yl)-1-isopropyl-1H-pyrazole-4-carboxamide (15i)*. Compound **13** (200 mg, 1.0 mmol) was converted to the target compound using general procedure A. The crude product was purified by flash column chromatography on silica gel (35% EtOAc/hexane to 70% EtOAc/hexane) to afford **15i** (68 mg, 26% over 2 steps) as a solid. ¹H NMR (400 MHz, CDCl₃) δ 9.33 (bs, 1H), 6.54 (s, 1H), 5.67 (bs, 2H), 5.37 (bs, 1H), 4.27 (sep, $J = 6.8$ Hz, 1H), 2.81 (q, $J = 7.6$ Hz, 2H), 1.49 (d, $J = 6.8$ Hz, 6H), 1.35 (t, $J = 7.6$ Hz, 3H); ¹³C NMR (100 MHz, CDCl₃) δ 174.02, 166.94, 158.78, 150.60, 136.79, 99.97, 95.66, 48.67, 21.35, 20.02, 11.61. LCMS (ESI) m/z : 264 [M+H]⁺.

4.1.8.10. *5-Amino-1-isopropyl-3-(5-isopropylisoxazol-3-yl)-1H-pyrazole-4-carboxamide (15j)*. Compound **13** (200 mg, 1.0 mmol) was converted to the target compound using general procedure A. The crude product was purified by flash column chromatography on silica gel (35% EtOAc/hexane to 70% EtOAc/hexane) to afford **15j** (64 mg, 23% over 2 steps) as a solid. ¹H NMR (400 MHz, CDCl₃) δ 9.35 (bs, 1H), 6.50 (d, $J = 0.8$ Hz, 1H), 5.67 (bs, 2H), 5.38 (bs, 1H), 4.26 (sep, $J = 6.4$ Hz, 1H), 3.15-3.05 (m, 1H), 1.49 (d, $J = 6.4$ Hz, 6H), 1.35 (d, $J = 7.2$ Hz, 6H); ¹³C NMR (100 MHz, CDCl₃) δ 177.87, 166.94, 158.59, 150.59, 136.84, 98.82, 95.64, 48.67, 27.03, 21.34, 20.79. LCMS (ESI) m/z : 278 [M+H]⁺.

4.1.8.11. *5-Amino-3-(5-(tert-butyl)isoxazol-3-yl)-1-isopropyl-1H-pyrazole-4-carboxamide (15k)*. Compound **13** (200 mg, 1.0 mmol) was converted to the target compound using general procedure A. The crude product was purified by flash column chromatography on silica gel (35% EtOAc/hexane to 70% EtOAc/hexane) to afford **15k** (61 mg, 21% over 2 steps) as a solid. ¹H NMR (400 MHz, CDCl₃) δ 9.36 (bs, 1H), 6.49 (s, 1H), 5.67 (bs, 2H), 5.37 (bs, 1H), 4.27 (sep, $J = 6.4$ Hz, 1H), 1.49 (d, $J = 6.4$ Hz, 6H), 1.38 (s, 9H); ¹³C NMR (100 MHz, CDCl₃) δ 180.35, 166.98, 158.47, 150.62, 136.87, 98.17, 95.61, 48.67, 32.67, 28.77, 21.32. LCMS (ESI) m/z : 292 [M+H]⁺.

4.1.8.12. *5-Amino-3-(5-cyclopropylisoxazol-3-yl)-1-isopropyl-1H-pyrazole-4-carboxamide (15l)*. Compound **13** (200 mg, 1.0 mmol) was converted to the target compound using general procedure A. The crude product was purified by flash column chromatography on silica gel (35% EtOAc/hexane to

70% EtOAc/hexane) to afford **15l** (66 mg, 24% over 2 steps) as a solid. ^1H NMR (400 MHz, CDCl_3) δ 9.29 (bs, 1H), 6.41 (s, 1H), 5.54 (bs, 1H), 4.25 (sep, $J = 6.8$ Hz, 1H), 2.08-2.01 (m, 1H), 1.45 (d, $J = 6.8$ Hz, 6H), 1.10-0.96 (m, 4H); ^{13}C NMR (100 MHz, CDCl_3) δ 174.18, 167.02, 158.89, 150.63, 136.71, 98.32, 95.49, 48.62, 21.37, 8.45, 7.87. LCMS (ESI) m/z : 276 $[\text{M}+\text{H}]^+$.

4.1.8.13. 5-Amino-3-(5-cyclohexylisoxazol-3-yl)-1-isopropyl-1H-pyrazole-4-carboxamide (15m). Compound **13** (200 mg, 1.0 mmol) was converted to the target compound using general procedure A. The crude product was purified by flash column chromatography on silica gel (35% EtOAc/hexane to 70% EtOAc/hexane) to afford **15m** (82 mg, 26% over 2 steps) as a solid. ^1H NMR (400 MHz, CDCl_3) δ 9.37 (bs, 1H), 6.50 (s, 1H), 5.69 (bs, 2H), 5.40 (bs, 1H), 4.27 (sep, $J = 6.8$ Hz, 1H), 2.81 (t, $J = 10.8$ Hz, 1H), 2.09 (d, $J = 13.2$ Hz, 2H), 1.83 (d, $J = 12.8$ Hz, 2H), 1.73 (d, $J = 12.4$ Hz, 1H), 1.50 (d, $J = 6.8$ Hz, 6H), 1.46 (s, 1H), 1.42 (s, 1H), 1.39 (s, 1H), 1.36-1.24 (m, 2H); ^{13}C NMR (100 MHz, CDCl_3) δ 176.93, 166.96, 158.63, 150.66, 136.96, 98.86, 95.83, 48.76, 36.21, 31.12, 25.81, 25.64, 21.28. LCMS (ESI) m/z : 318 $[\text{M}+\text{H}]^+$.

4.2. Kinase assay and profiling

Biochemical kinase assays and kinome profiling were performed by Reaction Biology Corp. (San Diego, CA). In biochemical kinase assays, inhibitory effects were determined using a mixture of ATP (10 μM) and RET enzymes (RET-WT, 2 nM; RET-V804M, 60 nM) in a 10-dose IC_{50} mode with 3-fold serial dilution starting at 10 μM of the test compounds. In kinase profiling, **15l** (1 μM) was used along with 10 μM ATP against 369 recombinant human kinases in duplicate mode.

4.3. Molecular modeling

The crystal structure of RET kinase in a complex with the inhibitor PP1 (Protein Data Bank (PDB) code 2IVV) [32] was used for docking simulations. The structure of the gatekeeper mutant (V804M) RET kinase was constructed using the rapid torsion scan tool in Maestro. Models of RET kinase inhibitors were constructed using Maestro build panel and minimized using the MacroModel of Maestro in the Schrödinger suite program. The RET kinase structure was minimized using the Protein Preparation Wizard by applying an OPLS-2005 force field [33]. After construction of the ligands and

proteins for docking, receptor-grid files were generated. Ligand docking into the ATP binding site of RET kinase was carried out using the Schrödinger docking program, Glide [34]. The energy minimized structures of RET kinase inhibitors were docked into the prepared receptor grid. The best-docked poses were selected as the lowest Glide score.

4.4. Cell culture

RET and RET-V804M transformed Ba/F3 cell lines were cultured in RPMI1640 (Welgene #LM011-01), supplemented with 10% fetal bovine serum (Hyclone), Antibiotic-Antimycotic solution (Welgene, #LS203-01) containing 10,000 U/mL penicillin, and 10 mg/mL streptomycin and 25 µg/mL amphotericinB in 0.85% NaCl. TT cells were grown in RPMI media, supplemented with 15% fetal bovine serum and 1% Antibiotic-Antimycotic solution. Nthy ori-3-1 cells were grown RPMI1640 media, supplemented with 10% FBS, 1% antibiotics, and 2 mM glutamine. The cells were maintained in a humidified atmosphere containing 5% CO₂ at 37 °C.

4.5. Cell viability assays

Cells (1×10^4) were plated in 96 well tissue culture plates. Each compound was added to each well at 8 dose points of 5-fold serial dilution in DMSO (1% DMSO). After treatment with each compound, CTG assay solution (Promega, G7572) was added to each well and plates were incubated for 72 h. Cell proliferation was assessed by measuring the luminescence using a 96 well plate reader (ENVISION).

4.6. Western blot analysis

Cells were harvested and lysed using IP buffer containing 50 mM HEPES (pH 7.4), 1% Triton X-100, 2 mM EDTA, 150 mM NaCl, 2.5 mM NaF, 5 mM Na₃VO₄, protease inhibitor cocktail tablet (Roche, #11-878-580-001). The protein concentration was determined by using the Bradford assay. Proteins were separated using SDS-PAGE and transferred onto PVDF membrane (Millipore, #IPVH00010). The membranes were blocked using 5% skim milk in TBS-T buffer. The rabbit polyclonal antibody against pRET (Y905, #3221, 1:1000), RET (#3220, 1:1000), pPLCγ (Y783, #2821, 1:1000), pShc

(Y317, #2431, 1:1000) was purchased from Cell Signaling Technologies, and the rabbit polyclonal antibody against pRET (Y1062, #sc-20252, 1:1000), PARP1/2 (H-250, sc-7150) and anti- β -actin (sc-47778, 1:1000) antibody was obtained from Santa Cruz Biotechnology. All primary antibodies were diluted in TBS-T at 1:1000. Each primary antibody was incubated overnight at 4 °C, followed by secondary antibody treatment for 1 h at room temperature. Secondary antibodies were purchased from Santa Cruz Technology. Proteins were detected using ECL substrate, and then exposed to an X-ray film.

4.7. Soft agar assay

Anchorage-independent growth was analyzed by using colony formation on soft agar. Equal volumes of agar (1%, DNA grade) and 2x RPMI (with 20% FBS) were mixed to generate a 0.5% base agar in a 6 well plate. Cells were suspended in 2xRPMI1640 (with 20% FBS) and 0.7% top agar, with a final concentration of 5×10^3 cells per well. The top agar was covered with compound-added media. The plates were incubated at 37 °C in a humidified atmosphere containing 5% CO₂ for 4 w and refreshed twice a week. Colonies were fixed and stained with 0.5 mL of 0.005% crystal violet in PBS for 45 min at room temperature.

Acknowledgments

This work was supported by Korea Institute of Science and Technology (KIST), and the KU-KIST Graduate School of Converging Science and Technology Program, a grant (D36403) of Korea Basic Science Institute, and Creative Fusion Research Program through the Creative Allied Project of the National Research Council of Science & Technology (CAP-12-1-KIST).

References

- [1] M. Huang, A.J. Shen, J. Ding, M.Y. Geng, Molecularly targeted cancer therapy: some lessons from the past decade, *Trends Pharmacol. Sci.* 35 (2014) 41-50.
- [2] W.W. Ma, A.A. Adjei, Novel Agents on the Horizon for Cancer Therapy, *CA-Cancer J Clin.* 59 (2009) 111-137.
- [3] C. Sun, R. Bernards, Feedback and redundancy in receptor tyrosine kinase signaling: relevance to cancer therapies, *Trends Biochem. Sci.* 39 (2014) 465-474.
- [4] J.D. Clark, M.E. Flanagan, J.B. Telliez, Discovery and Development of Janus Kinase (JAK) Inhibitors for Inflammatory Diseases, *J. Med. Chem.* 57 (2014) 5023-5038.
- [5] P.J. Barnes, New anti-inflammatory targets for chronic obstructive pulmonary disease, *Nat. Rev. Drug Discovery*, 12 (2013) 543-559.
- [6] A.S. Banks, F.E. McAllister, J.P.G. Camporez, P.J.H. Zushin, M.J. Jurczak, D. Laznik-Bogoslavski, G.I. Shulman, S.P. Gygi, B.M. Spiegelman, An ERK/Cdk5 axis controls the diabetogenic actions of PPAR gamma, *Nature* 517 (2015) 391-395.
- [7] L.M. Mulligan, RET revisited: expanding the oncogenic portfolio, *Nat Rev Cancer.* 14 (2014) 173-186.
- [8] F. Carlomagno, M. Santoro, Thyroid cancer in 2010: a roadmap for targeted therapies, *Nat Rev Endocrinol.* 7 (2011) 65-67.
- [9] N. Asai, T. Iwashita, M. Matsuyama, M. Takahashi, Mechanism of Activation of the Ret Protooncogene by Multiple Endocrine Neoplasia 2a Mutations, *Mol. Cell. Biol.* 15 (1995) 1613-1619.
- [10] A.N. Cranston, C. Carniti, K. Oakhill, E. Radzio-Andzelm, E.A. Stone, A.S. McCallion, S. Hodgson, S. Clarke, P. Mondellini, J. Leyland, M.A. Pierotti, J. Whittaker, S.S. Taylor, I. Bongarzone, B.A.J. Ponder, RET is constitutively activated by novel tandem mutations that alter the active site

resulting in multiple endocrine neoplasia type 2B, *Cancer Res.* 66 (2006) 10179-10187.

[11] S.D. Pandit, H. DonisKeller, T. Iwamoto, J.M. Tomich, L.J. Pike, The multiple endocrine neoplasia type 2B point mutation alters long-term regulation and enhances the transforming capacity of the epidermal growth factor receptor, *J. Biol. Chem.* 271 (1996) 5850-5858.

[12] Y.S. Ju, W.C. Lee, J.Y. Shin, S. Lee, T. Bleazard, J.K. Won, Y.T. Kim, J.I. Kim, J.H. Kang, J.S. Seo, A transforming KIF5B and RET gene fusion in lung adenocarcinoma revealed from whole-genome and transcriptome sequencing, *Genome Res.* 22 (2012) 436-445.

[13] F. Li, Y. Feng, R. Fang, Z.Y. Fang, J.F. Xia, X.K. Han, X.Y. Liu, H.Q. Chen, H.Y. Liu, H.B. Ji, Identification of RET gene fusion by exon array analyses in "pan-negative" lung cancer from never smokers, *Cell Res.* 22 (2012) 928-931.

[14] T. Kohno, H. Ichikawa, Y. Totoki, K. Yasuda, M. Hiramoto, T. Nammo, H. Sakamoto, K. Tsuta, K. Furuta, Y. Shimada, R. Iwakawa, H. Ogiwara, T. Oike, M. Enari, A.J. Schetter, H. Okayama, A. Haugen, V. Skaug, S. Chiku, I. Yamanaka, Y. Arai, S.I. Watanabe, I. Sekine, S. Ogawa, C.C. Harris, H. Tsuda, T. Yoshida, J. Yokota, T. Shibata, KIF5B-RET fusions in lung adenocarcinoma, *Nat Med.* 18 (2012) 375-377.

[15] K. Takeuchi, M. Soda, Y. Togashi, R. Suzuki, S. Sakata, S. Hatano, R. Asaka, W. Hamanaka, H. Ninomiya, H. Uehara, Y.L. Choi, Y. Satoh, S. Okumura, K. Nakagawa, H. Mano, Y. Ishikawa, RET, ROS1 and ALK fusions in lung cancer, *Nat Med.* 18 (2012) 378-381.

[16] F. Carlomagno, T. Guida, S. Anaganti, G. Vecchio, A. Fusco, A.J. Ryan, M. Billaud, M. Santoro, Disease associated mutations at valine 804 in the RET receptor tyrosine kinase confer resistance to selective kinase inhibitors, *Oncogene* 23 (2004) 6056-6063.

[17] L. Mologni, S. Redaelli, A. Morandi, I. Plaza-Menacho, C. Gambacorti-Passerini, Ponatinib is a potent inhibitor of wild-type and drug-resistant gatekeeper mutant RET kinase, *Mol. Cell. Endocrinol.* 377 (2013) 1-6.

- [18] H. Yoon, Y. Kwak, S. Choi, H. Cho, N.D. Kim, T. Sim, A Pyrazolo[3,4-*d*]pyrimidin-4-amine Derivative Containing an Isoxazole Moiety Is a Selective and Potent Inhibitor of RET Gatekeeper Mutants, *J. Med. Chem.* 59 (2016) 358-373.
- [19] F. Cameron, M. Sanford, Ibrutinib: First Global Approval, *Drugs.* 74 (2014) 263-271.
- [20] S. Sharma, J. Singh, R. Ojha, H. Singh, M. Kaur, P.M. Bedi, K. Nepali, Design strategies, structure activity relationship and mechanistic insights for purines as kinase inhibitors, *Eur. J. Med. Chem.* 112 (2016) 298-346.
- [21] Q.Y. Wang, Z.T. Zhang, X. Zhang, J. Zhang, Y. Kang, J.F. Peng, Synthesis of 7a-phenyl-1a,7a-dihydro-benzopyrano[2,3-*b*]azirin-7-ones via photoisomerization reaction, *RSC Adv.* 5 (2015) 4788-4794.
- [22] A. Maestro, J.M. Banez, J.A. Lopez, M.C. Romero-Avila, Use of 4-carbo-substituted isoxazoles in the polyhydroxylated chain extension of 2,3-O-isopropylidene-D-glyceraldehyde, *Synthesis* (1998) 1023-1028.
- [23] J.A. Fuentes, A. Maestro, A.M. Testera, J.M. Banez, Synthesis of optically active beta'-hydroxy-beta-enaminoketones via enzymatic resolution of carbinols derived from 3,5-disubstituted isoxazoles, *Tetrahedron: Asymmetry* 11 (2000) 2565-2577.
- [24] M. Nitta, T. Kobayashi, Reductive Ring-Opening of Isoxazoles with Mo(Co)₆ and Water, *J. Chem. Soc. Chem. Comm.* (1982) 877-878.
- [25] A.S. Kalgutkar, H.T. Nguyen, A.D.N. Vaz, A. Doan, D.K. Dalvie, In vitro metabolism studies on the isoxazole ring scission in the anti-inflammatory agent leflunomide to its active alpha-cyanoenol metabolite A771726: Mechanistic similarities with the cytochrome P450-catalyzed dehydration of aldoximes, *Drug Metab. Dispos.* 31 (2003) 1240-1250.
- [26] D. Zhang, N. Raghavan, S.Y. Chen, H.Y. Zhang, M. Quan, L. Lecureux, L.M. Patrone, P.Y.S. Lam, S.J. Bonacorsi, R.M. Knabb, G.L. Skiles, K. He, Reductive isoxazole ring opening of the

anticoagulant razaxaban is the major metabolic clearance pathway in rats and dogs, *Drug Metab. Dispos.* 36 (2008) 303-315.

[27] R. Schackel, B. Hinkelmann, F. Sasse, M. Kalesse, The Synthesis of Novel Disorazoles, *Angew. Chem., Int. Ed.* 49 (2010) 1619-1622.

[28] J.C. Barrish, J. Singh, S.H. Spergel, W.C. Han, T.P. Kissick, D.R. Kronenthal, R.H. Mueller, Cupric Bromide Mediated Oxidation of 4-Carboxyoxazolines to the Corresponding Oxazoles, *J. Org. Chem.* 58 (1993) 4494-4496.

[29] Z.S. Zhang, K.K. Ojo, R. Vidadala, W.L. Huang, J.A. Geiger, S. Scheele, R. Choi, M.C. Reid, K.R. Keyloun, K. Rivas, L.K. Siddaramaiah, K.M. Comess, K.P. Robinson, P.J. Merta, L. Kifle, W.G.J. Hol, M. Parsons, E.A. Merritt, D.J. Maly, C.L.M.J. Verlinde, W.C. Van Voorhis, E.K. Fan, Potent and Selective Inhibitors of CDPK1 from *T. gondii* and *C. parvum* Based on a 5-Aminopyrazole-4-carboxamide Scaffold, *ACS Med. Chem. Lett.* 5 (2014) 40-44.

[30] E.S. Kim, H.S. Kim, J.N. Kim, An efficient Pd-catalyzed hydration of nitrile with acetaldoxime, *Tetrahedron Lett.* 50 (2009) 2973-2975.

[31] P. Diner, J.P. Alao, J. Soderlund, P. Sunnerhagen, M. Grotli, Preparation of 3-Substituted-1-Isopropyl-1*H*-pyrazolo[3,4-*d*]pyrimidin-4-amines as RET Kinase Inhibitors, *J. Med. Chem.* 55 (2012) 4872-4876.

[32] P.P. Knowles, J. Murray-Rust, S. Kjaer, R.P. Scott, S. Hanrahan, M. Santoro, C.F. Ibanez, N.Q. McDonald, Structure and chemical inhibition of the RET tyrosine kinase domain, *J. Biol. Chem.* 281 (2006) 33577-33587.

[33] D. Shivakumar, J. Williams, Y.J. Wu, W. Damm, J. Shelley, W. Sherman, Prediction of Absolute Solvation Free Energies using Molecular Dynamics Free Energy Perturbation and the OPLS Force Field, *J. Chem. Theory Comput.* 6 (2010) 1509-1519.

[34] R.A. Friesner, R.B. Murphy, M.P. Repasky, L.L. Frye, J.R. Greenwood, T.A. Halgren, P.C.

Sanschagrin, D.T. Mainz, Extra precision glide: Docking and scoring incorporating a model of hydrophobic enclosure for protein-ligand complexes, *J. Med. Chem.* 49 (2006) 6177-6196.

ACCEPTED MANUSCRIPT

Highlights

Novel 5-aminopyrazole-4-carboxamide derivatives were synthesized as RET inhibitors.

Compound 151 is potent on V804M-RET as well as on wt-RET.

Compound 151 is metabolically stable.

Compound 151 displays exceptional kinase selectivity.

Compound 151 suppresses growth of wt-RET-Ba/F3 and V804M-RET-Ba/F3 cells.

ACCEPTED MANUSCRIPT